catalysts

MDPI

Article

Hydrogen Production through Oxidative Steam Reforming of Acetic Acid over Ni Catalysts Supported on Ceria-Based Materials

Pedro J. Megía *, Anabel Morales, Arturo J. Vizcaíno, José A. Calles * and Alicia Carrero

Chemical and Environmental Engineering Group, Rey Juan Carlos University, c/Tulipán s/n, 28933 Móstoles, Spain

* Correspondence: pedro.megia@urjc.es (P.J.M.); joseantonio.calles@urjc.es (J.A.C.)

Abstract: Oxidative steam reforming allows higher energy efficiency and lowers coke deposition compared to traditional steam reforming. In this work, CeO_2-based supports have been prepared with Ni as the active phase, and they were tested in the oxidative steam reforming of acetic acid. The influence of the O_2/AcOH molar ratio (0–0.3) has been evaluated over Ni/CeO_2. The results stated that by increasing oxygen content in the feeding mixture, acetic acid conversion increases, too, with a decrease in coke deposition and hydrogen yield. To have a proper balance between the acetic acid conversion and the hydrogen yield, an O_2/AcOH molar ratio of 0.075 was selected to study the catalytic performance of Ni catalysts over different supports: commercial CeO_2, a novel mesostructured CeO_2, and CeO_2-SBA-15. Due to higher Ni dispersion over the support, the mesostructured catalysts allowed higher acetic acid conversion and hydrogen yield compared to the nonporous Ni/CeO_2. The best catalytic performance and the lowest coke formation (120.6 $mg_{coke} \cdot g_{cat}^{-1} \cdot h^{-1}$) were obtained with the mesostructured Ni/CeO_2. This sample reached almost complete conversion (>97%) at 500 °C, maintaining the hydrogen yield over 51.5% after 5 h TOS, being close to the predicted value by the thermodynamic equilibrium that is due to the synergistic coordination between Ni and CeO_2 particles.

Keywords: hydrogen production; oxidative reforming; catalysis; SBA-15; mesoporous ceria; nanocasting

Citation: Megía, P.J.; Morales, A.; Vizcaíno, A.J.; Calles, J.A.; Carrero, A. Hydrogen Production through Oxidative Steam Reforming of Acetic Acid over Ni Catalysts Supported on Ceria-Based Materials. *Catalysts* **2022**, *12*, 1526. https://doi.org/10.3390/catal12121526

Academic Editor: Paraskevi Panagiotopoulou

Received: 29 October 2022
Accepted: 24 November 2022
Published: 27 November 2022

1. Introduction

Substantial growth in population and economic development are the main reasons for the energy demand rise [1,2]. This demand is mainly covered by fossil fuels, resulting in about 830 million tons of CO_2 emissions per year [3]. Against fossil fuels, hydrogen, which is considered the energy vector of the future, could replace them and reduce the related carbon emissions [4]. In 2020, 90 Mt of hydrogen was produced worldwide, mainly from thermochemical processes using fossil fuels [5]. As the sustainability of hydrogen is related to the cleanness of the hydrogen production pathway and the energy used during its obtention, biomass-to-hydrogen processes have gained attention in the last few years [6,7]. More specifically, the combination of the thermochemical conversion of biomass, followed by the reforming process of the produced oil, is a promising alternative [8–10]. Bio-oil is a complex mixture of different oxygenated hydrocarbons (carboxylic acids, ketones, phenols, and aldehydes among others [11]) that could be separated into an organic fraction and an aqueous fraction. The aqueous fraction is composed of different water-soluble compounds with variable concentrations, where acetic acid is usually one of the major compounds [9,12,13]. Bio-oil aqueous fraction steam reforming has been studied as a viable alternative for producing green hydrogen from biomass [6,14,15]. However, this process has some limitations that are due to the catalyst deactivation primarily produced from coke deposition and because the primary reaction is highly endothermic [16,17]. On the contrary, oxidative steam reforming, which implies the co-feeding of oxygen, has been less reported on despite its higher energy efficiency, given that the oxidation reactions can supply part of the energy required for the endothermic reactions. Moreover, it also

allows delaying catalyst deactivation by favoring the combustion of carbon deposits [18,19]. Notwithstanding the benefits of adding oxygen, the main drawbacks of oxidative steam reforming are the lower hydrogen selectivity and catalyst deactivation by the metallic, active phase oxidation; thus, the oxygen/steam ratio should be controlled [20]. The overall reaction that described this process is summarized in Equation (1).

$$C_nH_mO_K + pO_2 + (2n - k - 2p)H_2O \rightarrow nCO_2 + \left(2n + \frac{m}{2} - k - 2p\right)H_2 \quad (1)$$

Apart from that, it is well-known that the catalyst also plays a crucial role in the reforming processes [21]. This is why many researchers focus on catalyst formulation, being that Ni-based catalysts are the most studied [19,22] given their ability to crack C-C and C-H bonds [23], which is necessary according to the mechanism described in the literature that is represented in Scheme 1.

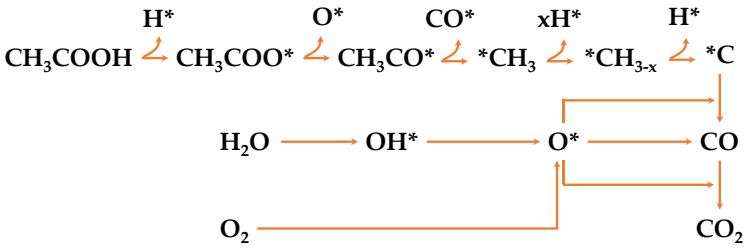

Scheme 1. Mechanism of the oxidative steam reforming of acetic acid. Adapted from [24].

As support, ceria has been reported to have high oxygen mobility, which can reduce the formation of carbon deposits over the active sites [25]. Unfortunately, the nonporous structure with a low surface of ceria area has limited its application as a support in reforming reactions [26]. However, by modifying its physical properties related to geometrical features including size, dimension, orientation, and morphology, it is possible to enhance its catalytic role by decreasing the coke formation and inhibiting the deactivation caused by metal sintering. Therefore, the control of the support morphology plays a key crucial role in improving the catalytic activity since it can facilitate the formation of oxygen vacancies [26] and also influence the formation of metal species ascribed to the Ce^{3+}/Ce^{4+} redox properties of CeO_2 [27]. Moreover, the high surface area of ceria allows better Ni-species dispersion because of the smaller crystallite size, thus strengthening the interaction between Ni and CeO_2 and promoting Ni reducibility, which may result in a better catalytic performance [26]. Despite this, a ceria-based porous structure with a high surface area used as support for reforming purposes is rarely reported. Preparing mesoporous ceria would allow taking advantage of the oxygen mobility of CeO_2 but also the reaching of higher metal dispersion on a support with a higher surface area, as reported before [28]. To the best of our knowledge, no papers have been published on acetic acid oxidative steam reforming using ceria-based mesoporous structures as support. Thus, this work aims to study the influence of different CeO_2-based supports: a novel mesostructured CeO_2 prepared by nanocasting, a commercial CeO_2, and CeO_2-SBA-15 on the activity and hydrogen selectivity during the oxidative steam reforming of acetic acid as a bio-oil aqueous fraction model compound using Ni as the active phase.

2. Results and Discussion

2.1. Catalysts Characterization

Nitrogen adsorption–desorption isotherms of the prepared porous catalysts and the supports are displayed in Figure 1, except for the commercial CeO_2 given its nonporous structure. As can be discerned, all the porous samples showed a type IV isotherm according to the IUPAC classification characteristic of mesoporous materials with an H1 and H3-hysteresis loop for SBA-15-based samples and mesoporous cerium-based materials, respectively. While the H1 hysteresis loop indicates the presence of a well-ordered hexagonal

mesoporous structure characteristic of SBA-15 materials [15], H3-type hysteresis loops are known for not having any limitation adsorption at high P/P_0, typical of layered particles that give rise to porosity [29]. These results agree with the structure observed by TEM for the SBA-15 and CeO_2-m supports displayed in Figure 2a,b, respectively.

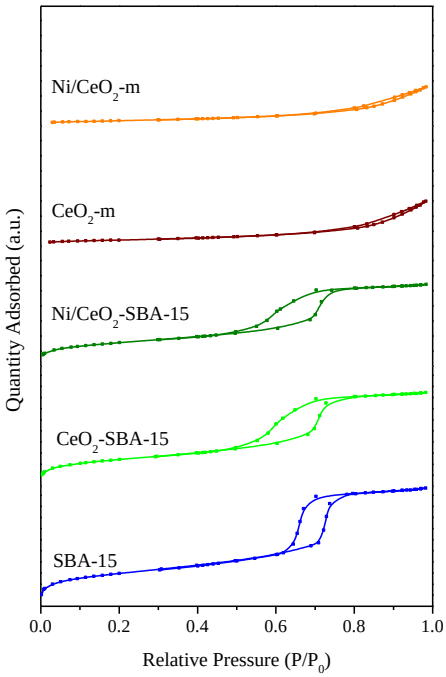

Figure 1. Nitrogen adsorption–desorption isotherms for the prepared Ni-based catalysts.

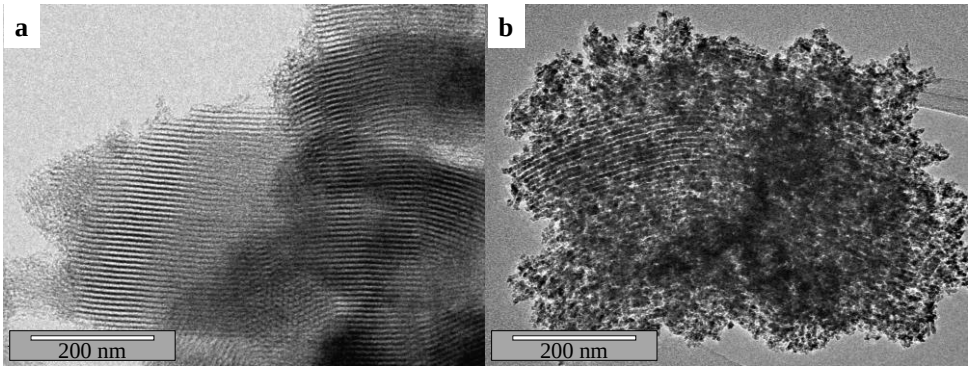

Figure 2. TEM micrographs of calcined (**a**) SBA-15 and (**b**) CeO_2-m supports.

The physicochemical properties of the supports and the catalysts used in this work are summarized in Table 1. The metal loadings, determined by ICP-AES analysis, were close to the nominal values fixed during the catalyst synthesis. Attending to BET surface area values, SBA-15-based materials achieved the highest values despite this value decreasing when Ni is incorporated into the support during the synthesis step as reported before [30]. Ce-based catalysts, more specifically the CeO_2-m sample, exhibit similar BET surfaces and pore volume rates than those described in the literature for similar materials prepared by nanocasting using this template [31,32]. However, this support presents a lower surface area when compared to the template used during the synthesis (SBA-15). Roggenbuck et al. [31] ascribed this reduction to the differences between the density of the bulk phases (SiO_2 and CeO_2) and the microporosity present in SBA-15, which significantly contributes to its specific surface area. Instead, commercial CeO_2 has a nonporous structure [26].

Table 1. Physicochemical properties of synthesized supports and catalysts.

Sample	Ni[a] (wt.%)	Ce[a] (wt.%)	S_{BET} (m^2/g)	V_p[b] (cm^3/g)	D_p[c] (nm)	D_{NiO}[d] (nm)	D_{Ni}[e] (nm)
CeO_2	-	-	-	-	-	-	-
Ni/CeO_2	6.2	-	-	-	-	32.5	28.4
CeO_2-m	-	-	114	0.29	7.3	-	-
Ni/CeO_2-m	6.7	-	98	0.26	8.1	12.5	12.2
SBA-15	-	-	601	0.91	7.7	-	-
CeO_2-SBA-15	-	9.1	490	0.72	7.2	-	-
Ni/CeO_2-SBA-15	6.3	8.5	432	0.63	7.3	11.2	11.0

[a] Determined by ICP-AES in calcined samples; [b] pore volume measured at $P/P_0 = 0.97$; [c] BJH desorption average pore diameter; [d] mean crystallite size determined from XRD pattern of calcined catalysts using the Scherrer equation in the (200) diffraction line of NiO; [e] mean crystallite size determined from XRD pattern of reduced catalysts using the Scherrer equation in the (111) diffraction line of Ni.

Figure 3 shows the XRD diffractograms of the calcined catalysts. On the one hand, peaks arise in all the samples at 28.5, 33, 47.3, 56.1, 69.4, 76.7, and 79.1°, corresponding to cubic CeO_2 (JCPDS 01-089-8436), these peaks being more intense in the commercial CeO_2 support given its higher crystallinity. In the case of Ni/CeO_2-SBA-15, these peaks evidence that CeO_2 is in the form of crystallites distributed over the SBA-15 not being completely dispersed, with unlikely interaction with the Ni phase [33]. On the other hand, peaks at 37.3, 43.4, and 63° can also be discerned from the presence of cubic NiO (JCPDS 01-075-0197). The low relative of NiO peaks in Ni/CeO_2 is due to the high intensity of CeO_2 diffraction lines making them difficult to be clearly observed. Broadly, in the Ni/CeO_2-m and Ni/CeO_2-SBA-15 samples, these peaks are broader when compared to Ni/CeO_2, indicating smaller crystallite size. This is ascribed to the high surface area of the mesostructured supports, which allows better distribution of Ni species on the carrier. Therefore, it is reasonable that the mean crystallite sizes calculated by applying the Scherrer equation on the (200) diffraction plane of cubic NiO pattern for these samples were around 60% smaller than that obtained for Ni/CeO_2 (see Table 1).

The reducibility of the prepared catalysts was evaluated through H_2-TPR analysis, whose profiles are represented in Figure 4. In all the samples, two main features could be distinguished at temperatures below 500 °C, ascribed to the reduction in NiO species with different degrees of interaction with the support. Samples supported on ceria show similar profiles where another peak at higher temperatures (740–805 °C) can also be discerned. According to what is described in the literature, this peak is assigned to the reduction of Ce^{4+} to Ce^{3+} in bulk ceria [34,35]. The differences between the reduction temperatures of NiO particles are related to lower crystallite sizes found over Ni/CeO_2-m than over the commercial CeO_2. On the other side, the reduction profile of the Ni/CeO_2-SBA-15 sample is similar to that of Ni/SBA-15 described elsewhere [36] but shifted to lower temperatures ascribed to the presence of cerium in the sample [37].

After the activation step to reduce the NiO species, all the catalysts were again characterized by XRD whose diffractograms are displayed in Figure 5. As can be observed, no diffraction lines of the NiO pattern could be distinguished. On the contrary, diffraction lines of cubic Ni^0 (JCPDS 01-071-3740) arise at 44.6 and 51.8, stating that the reduction step was successful, being that all the Ni-oxides were reduced to the metallic state. No diffraction peaks corresponding to metallic Ce could be observed since Ce oxides need higher reduction temperatures, above 1000 °C [38]. As happened with calcined samples, the Ni/CeO_2-m and Ni/CeO_2-SBA-15 samples present broader peaks than the nonporous Ni/CeO_2, resulting in lower mean crystallite size calculated using the Scherrer equation from the (111) diffraction plane of Ni^0 (see Table 1), as a consequence of the higher surface area in the supports.

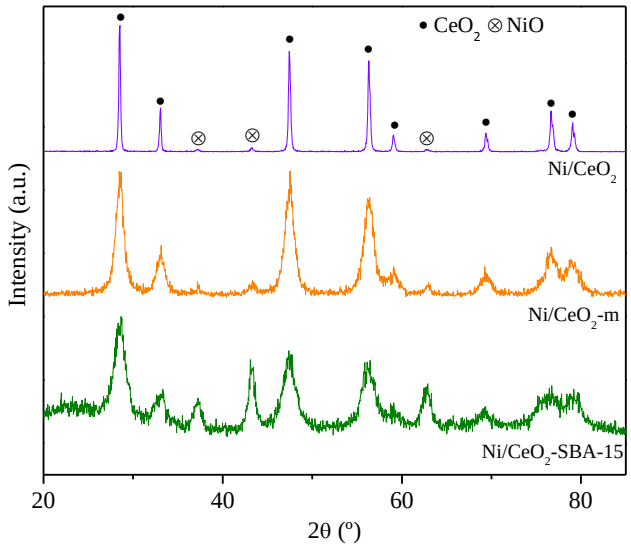

Figure 3. XRD patterns of calcined Ni-based catalysts.

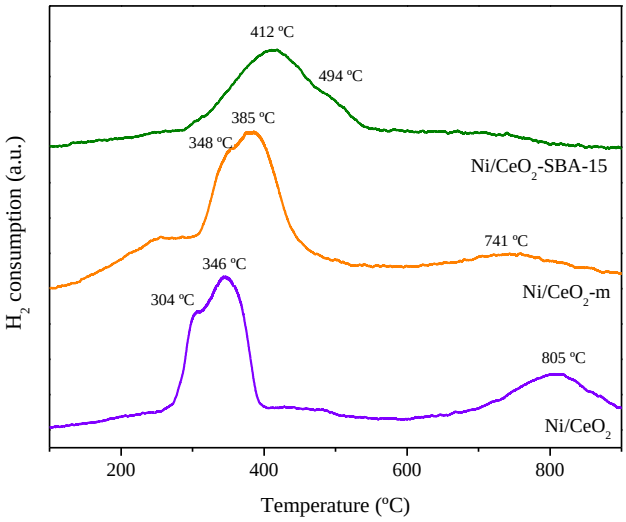

Figure 4. H_2-TPR profiles of calcined Ni-based catalysts.

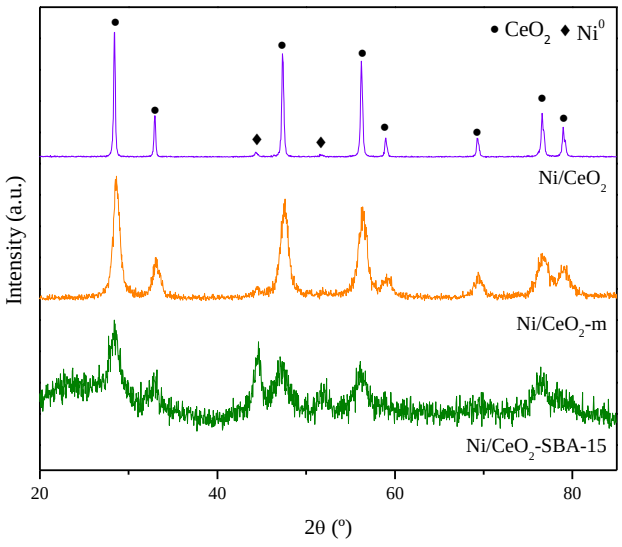

Figure 5. XRD patterns of reduced Ni-based catalysts.

2.2. Catalytic Performance

The influence of the O_2/AcOH molar ratio in hydrogen production by acetic acid steam reforming was evaluated with the Ni/CeO_2 catalyst at 500 °C. This temperature was selected to work in mild temperature conditions, more favorable from an energetic point of view, in which coke formation is favored to observe apparent differences between the O_2/AcOH molar ratios used. The O_2/AcOH molar ratios were 0, 0.03, 0.075, 0.15, and 0.3. The results obtained after 5 h time-on-stream are shown in Figure 6. When oxygen content increases, acetic acid conversion increases along with a decrease in coke deposition and hydrogen yield. Compared to the conventional steam reforming (O_2/AcOH = 0), the reaction using the highest O_2/AcOH molar ratio (0.3) achieved a 16% higher acetic acid conversion value and a decrease of about 90 $mg_{coke} \cdot g_{cat}{}^{-1} \cdot h^{-1}$, which implies a 40% reduction in the coke deposition rate. These results underline the benefits of increasing the oxygen ratio during the reaction. Still, it should also be highlighted that the hydrogen yield decreases by 8%, which is one of the main drawbacks of including oxygen in the feed mixture. The obtained results are entirely in line with those reported by Batista da Silva et al. [39], in which they study the effect of the O_2/AcOH molar ratio from a thermodynamic point of view. To maximize hydrogen production, it is mandatory to control the oxygen addition to take advantage of oxidative reforming while maintaining the hydrogen yield as high as possible. Despite the acetic acid conversion following a rising trend, it could be appreciated how the amount of coke deposited remains almost constant at an O_2/AcOH molar ratio $\geq$ 0.075. At the same time, with a 0.075 O_2/AcOH molar ratio, hydrogen yield decreases by only 2.4% compared to conventional steam reforming. For that reason, to have a proper balance between the oxygen fed and the hydrogen produced, this ratio (O_2/AcOH = 0.075) was fixed from now on.

Then, the catalytic performance of Ni/CeO_2, Ni/CeO_2-SBA-15, and Ni/CeO_2-m was evaluated using an O_2/AcOH molar ratio = 0.075. In this sense, results in terms of acetic acid conversion and hydrogen yield along TOS are displayed in Figure 7. On the one hand, attending to acetic acid conversion (Figure 7a), the Ni/CeO_2 sample reached lower conversion values than the other samples, and deactivation with time was evidenced by the decrease in conversion from 81.3% to 70.2% after 5 h TOS. Despite the presence of CeO_2 in the catalyst formulation reported to promote coke gasification being active in water-gas shift reaction [40], this behavior could be ascribed to the Ni/CeO_2 nonporous structure, resulting in a low active phase dispersion over the support as a consequence of low surface area. This statement agrees with the highest Ni mean crystallite size determined by the Scherrer equation (see Table 1).

Ni/CeO_2-SBA-15 and Ni/CeO_2-m reached almost complete conversion at short TOS, but the Ni/CeO_2-SBA-15 sample decreased conversion values when TOS is above 3 h. However, Ni/CeO_2-m presents high stability, maintaining the acetic acid conversion at around 97%, at least during the 5 h of TOS. Since Ni mean crystallite sizes were similar for both samples, this behavior could be ascribed to differences in the support behavior. The lower CeO_2 content in the SBA-15-based sample does not have as much oxygen mobility as Ni/CeO_2-m and thus does not promote the coke gasification to a greater extent. In this line, Bereketidou et al. [41] studied the effect of CeO_2 content (0, 10, and 20 wt.%) in the support of Ni-based catalysts for biogas reforming. They reported that doping a 20 wt.% of CeO_2 to Ni/Al_2O_3 provided higher reforming activity and hydrogen yield compared to the unpromoted sample while suppressing carbon formation attributed to the redox properties of ceria. Equally, Santos et al. [42] reported a similar behavior in the partial oxidation of methane using Pt/CeO_2/Al_2O_3 catalysts. They evaluated the effect of CeO_2 addition ranging from 1 to 20 wt.%, leading to the conclusion that catalysts with higher CeO_2 loadings were more resistant to coke deposition given the oxygen exchange capacity of ceria to store/release oxygen because of the Ce^{4+}/Ce^{3+} redox couple. On the other hand, hydrogen yield followed a similar trend to conversion for the structured catalysts, being higher than the hydrogen yield achieved with the nonporous sample. Ni/CeO_2-SBA-15 and Ni/CeO_2-m reached higher hydrogen yields compared to Ni/CeO_2, ascribed to smaller Ni

crystallites, which may lead to more available active sites. Whereas the Ni/CeO_2-m sample showed higher stability given the almost constant value of hydrogen yield obtained, being close to the value expected in the thermodynamic equilibrium, Ni/CeO_2-SBA-15 revealed clear deactivation with TOS.

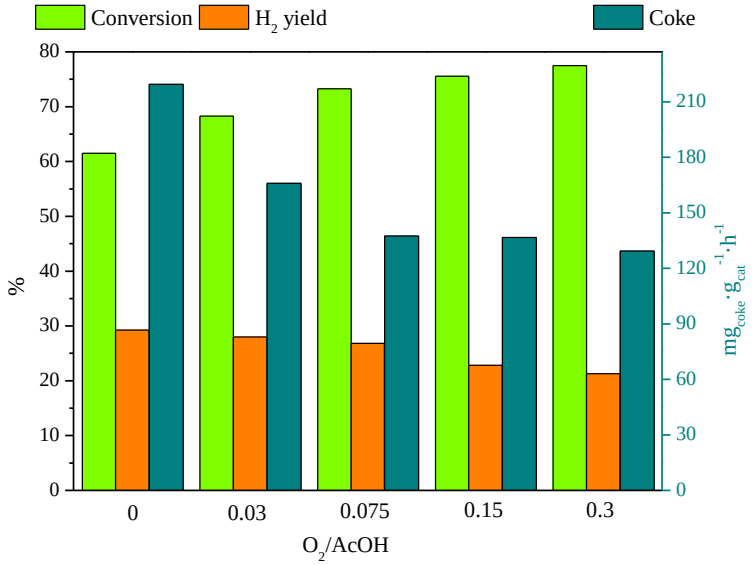

Figure 6. Catalytic results in terms of conversion, hydrogen yield, and coke deposition for different O_2/AcOH molar ratios (0–0.3) at 500 °C after 5 h TOS for Ni/CeO_2.

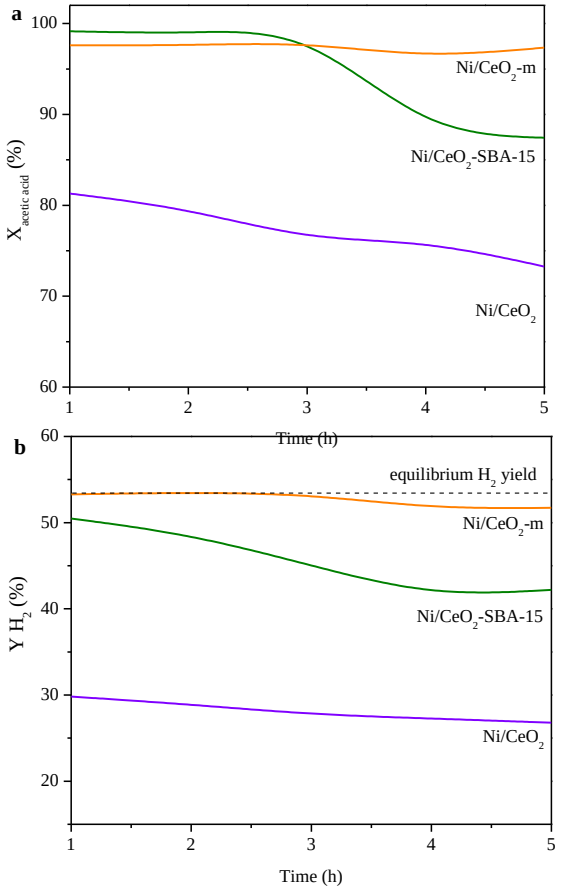

Figure 7. Catalytic results of Ni-supported catalysts at 500 °C using an O_2/AcOH molar ratio of 0.075: (**a**) acetic acid conversion; (**b**) hydrogen yield.

Coke formation has been reported to be one of the main causes of deactivation in reforming catalysts [14,43,44], not only referring to the amount of coke deposited but also related to its nature. Thus, coke deposited during the oxidative steam reforming of acetic acid was characterized by means of TGA analysis to the used samples, performed under an air-flowing atmosphere. In this context, the derivative thermogravimetric profiles are displayed in Figure 8 where the amount of coke deposited in terms of $mg_{coke} \cdot g_{cat}^{-1} \cdot h^{-1}$ has been included. Broadly, all the profiles have a maximum in the range of 500–600 °C, which could be ascribed to the formation of carbon nanofibers with different ordering degrees given that the amorphous carbon is more reactive in reactions with O_2 oxidizing at temperatures below 400 °C [45]. Concerning all the curves, the maximum in the oxidizing temperature increases in the following order: Ni/CeO_2-m < Ni/CeO_2 < Ni/CeO_2-SBA-15, denoting that more condensed coke deposits have been formed with Ni/CeO_2-SBA-15, being thus more difficult to remove by air combustion [14]. This could also explain the higher coke production obtained for this sample. On the contrary, Ni/CeO_2-m reached the lowest temperature, near 500 °C, related to the more defective carbon nanofilaments, thus being more easily gasified during the reforming.

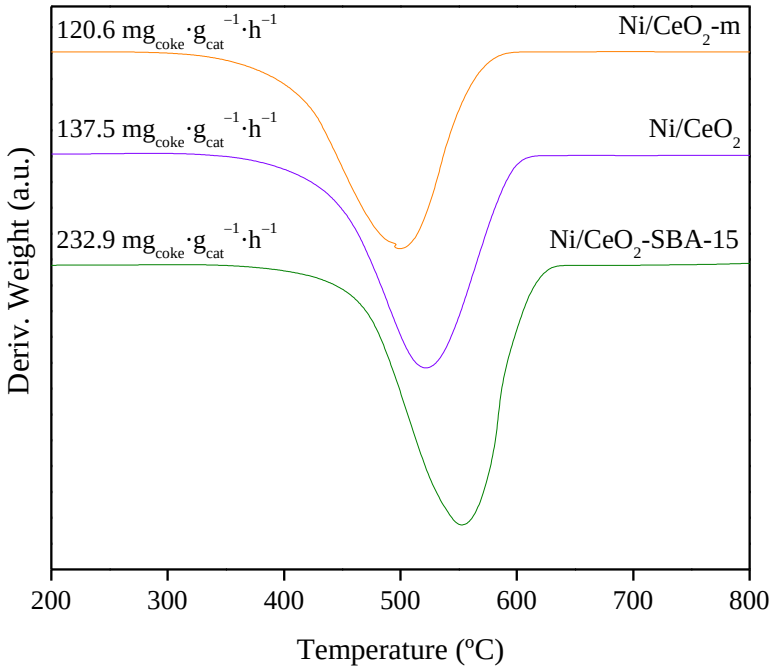

Figure 8. DGT curves of used Ni-supported CeO_2-based catalysts and coke amount deposited at 500 °C.

As stated before, apart from coke formation as a cause of deactivation, oxygen in the feed mixture could lead to active phase oxidation, leading to non-active sites [20]. In this regard, XRD analyses were performed on the used catalysts, whose diffractograms are represented in Figure 9. Peaks corresponding to graphitic carbon (JCPDS 00-041-1487) at 26.5° can be distinguished as a consequence of carbon deposition during the acetic acid oxidative steam reforming. This peak is more pronounced in the Ni/CeO_2-SBA-15 sample, according to higher coke deposition. These peaks could not be clearly discerned in the case of Ni/CeO_2, given the intensity of CeO_2 peaks. Peaks ascribed to cubic Ni^0 (JCPDS 01-071-3740) arise in all the samples at 44.6 and 51.8°, as most Ni species are under a reduced state during the whole reaction. Unlike the other samples, Ni/CeO_2-SBA-15 also exhibits peaks at 37.3, 43.4, and 63° because of the presence of cubic NiO (JCPDS 01-075-0197), indicating that apart from having the highest coke deposition value, the oxidation of the Ni^0 sites is taking place, which also contributes to catalyst deactivation, thus explaining the conversion and hydrogen yield drops observed in Figure 7.

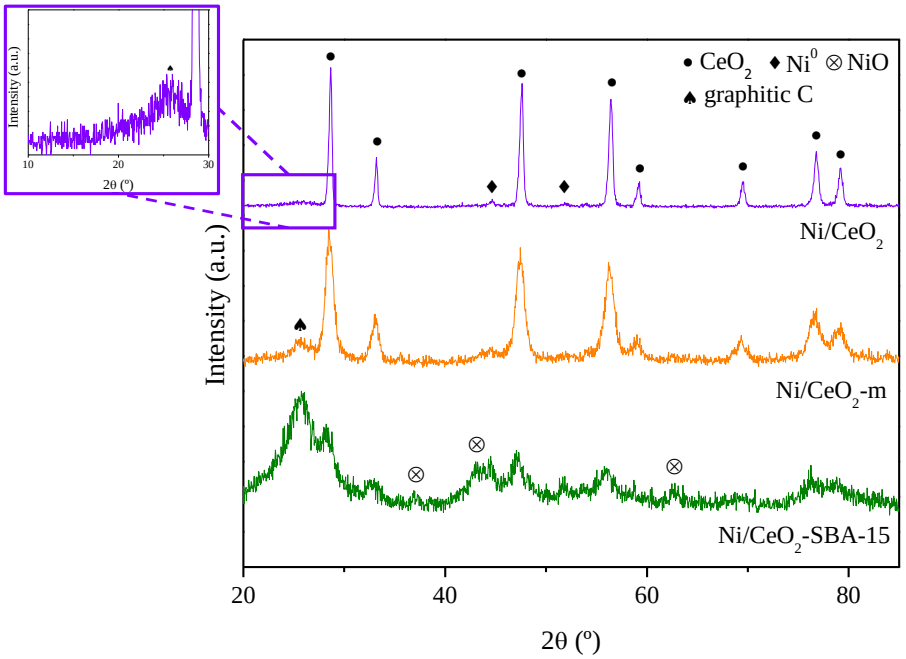

Figure 9. XRD patterns of spent Ni-base CeO_2-supported catalysts after 5 h TOS at 500 °C.

In summary, higher conversions and hydrogen yields were achieved with the catalysts with porous structures ascribed to the better dispersion of Ni species given their higher surface area to allow smaller crystallites size. When referred to coke, the samples with higher CeO_2 content present lower coke formation because of the promoting effect of CeO_2 toward carbon gasification. It is noteworthy that the carbon deposition over Ni/CeO_2-SBA-15 was almost two times higher compared to the other samples, which could explain the acetic acid conversion drop since coke is known to be one of the main causes of deactivation in Ni catalyst along with the active phase oxidation. In light of the above, mesostructured Ni/CeO_2-m was the catalyst with the best catalytic performance reaching the highest conversion and hydrogen yield and the lowest carbon deposition.

3. Materials and Methods

3.1. Supports and Catalysts Preparation

A series of Ni catalysts were prepared using different cerium-based supports. Three supports were employed: commercial cerium oxide (Scharlau), CeO_2-modified SBA-15, and mesostructured CeO_2. The commercial CeO_2 sample was treated by air calcination at 550 °C for 5 h with a heating rate of 1.8 °C/min. The SBA-15 material was prepared following a hydrothermal method described by Zhao et al. [46] using Pluronic 123 and TEOS surfactant and silica precursor, respectively. The as-synthesized sample was then calcined at 550 °C for 5 h at a heating rate of 1.8 °C/min to remove the templating agent. This SBA-15 silica was used to prepare the CeO_2-modified SBA-15 support (denoted as CeO_2-SBA-15) and the mesostructured ceria (CeO_2-m). In the first case, SBA-15 was subjected to incipient wetness impregnation using $Ce(NO_3)_3 \cdot 6H_2O$ as the precursor for achieving a 10 wt.% loading of Ce in the calcined support. On the other hand, the ordered mesoporous ceria (CeO_2-m) was prepared by nanocasting, as described elsewhere [47–52]. More specifically, in this work, SBA-15, as a mesoporous hard template, was filled with $Ce(NO_3)_3 \cdot 6H_2O$ as the metal precursor. For this purpose, 4.85 g of cerium nitrate was dissolved in 50 mL of pure ethanol after progressively adding 6 g of SBA-15 to achieve a homogeneous mixture. The mixture was stirred at room temperature until complete ethanol evaporation. Then, the SBA-15 filled with cerium nitrate was calcined at 600 °C for 6 h with a heating rate of 1.8 °C/min to get cerium oxide. This procedure was repeated three times to ensure the complete filling of the SBA-15 pores. To remove the SBA-15 used as the template, the sample was washed

with an aqueous NaOH solution and kept under stirring for 4 h at 60 °C. Then, mesoporous cerium particles were recovered by filtration and subsequently calcined at 550 °C.

The incorporation of Ni onto the three supports mentioned above was accomplished by using an aqueous solution of $Ni(NO_3)_2 \cdot 6H_2O$ to get Ni loadings around 7 wt.% in the final catalysts following the incipient wetness impregnation technique that was followed for CeO_2-SBA-15 [37]. However, with commercial CeO_2 and CeO_2-m, the wet impregnation method was used because of their low total pore volumes. Wet impregnation was done by adding 1.4 g of CeO_2 or CeO_2-m to the precursor solution (0.52 g of nickel nitrate dissolved in 5 mL of water) under stirring. Next, the mixture was aged in a rotary evaporator for 4 h. Finally, all samples were calcined at 550 °C for 5 h.

3.2. Supports and Catalysts Characterization

Textural properties of the prepared materials were determined using nitrogen adsorption–desorption isotherms at 77 K on a Micromeritics TRISTAR 3000 sorptometer. Before analysis, the samples were outgassed under vacuum at 200 °C for 4 h. Whereas surface area was calculated according to the Brunauer–Emmett–Teller method (BET), pore diameter was derived from the desorption isotherm applying the Barrett–Joyner–Halenda method (BJH). The calcined samples were dissolved by acidic digestion and measured in a Varian Vista-PRO AX CCD-Simultaneous ICP-AES spectrophotometer to have information about the metallic content. TEM micrographs were acquired on a high-resolution transmission electron microscope JEOL JEM-F200 (200 kV). The XRD technique was used to determine the crystalline phases in the samples according to the JCPDS index from the ICSD database using POWD-12++ software and the mean crystallite sizes were determined by the Scherrer equation. The corresponding diffractograms were acquired using a Philips X'pert PRO diffractometer using Cu Kα radiation. The samples' reducibility and metal-support interactions were studied using TPR analysis on a Micromeritics Autochem 2910 system. The experiments were carried out in situ under a reducing gas mixture (10% H_2/Ar) by flowing 35 N mL/min through the sample with a heating rate of 5 °C/min up to 980 °C. Samples were previously outgassed under Ar flow at 110 °C for 30 min. Thermogravimetric analyses were performed to evaluate the amount of carbon deposited during catalytic tests. These tests were done in air flow with a heating rate of 5 °C/min up to 1000 °C on a TGA-DSC Mettler Toledo thermobalance.

3.3. Catalytic Tests

The prepared catalyst activity in the acetic acid oxidative steam reforming was accomplished on a Microactivity-Pro unit provided by PID Eng & Tech. S.L. The equipment consists of a stainless steel fixed-bed tubular reactor (i.d. = 9.2 mm, L = 300 mm) placed inside an electric oven, as schematized in Figure 10. The temperature inside the reactor is measured using a K-thermocouple. All the components are located inside a stainless-steel hot box with a convector of hot air at 200 °C to avoid condensation of volatile products in the pipes and to allow the preheating of the reactants. The reactor outlet has a Peltier effect unit to condense and separate condensable vapors.

The reactions were performed isothermally at 500 °C and atmospheric pressure. Before, all the catalysts were in situ reduced under flowing pure hydrogen (30 mL/min) at 600 °C for 5.5 h with a heating rate of 2 °C/min according to H_2-TPR results. The reaction feed is a mixture containing acetic acid (AcOH) and water (S/C =2), which is pumped at a flow rate of 0.075 mL/min, vaporized at 200 °C, and mixed with different oxygen–nitrogen mixtures while maintaining the total gas flow at 60 mL/min to achieve a GHSV of 11,000 h^{-1}. The oxygen flow rate was fixed to get the O_2/AcOH molar ratios between 0 (steam reforming) and 0.3 (autothermal reforming of acetic acid [53,54]).

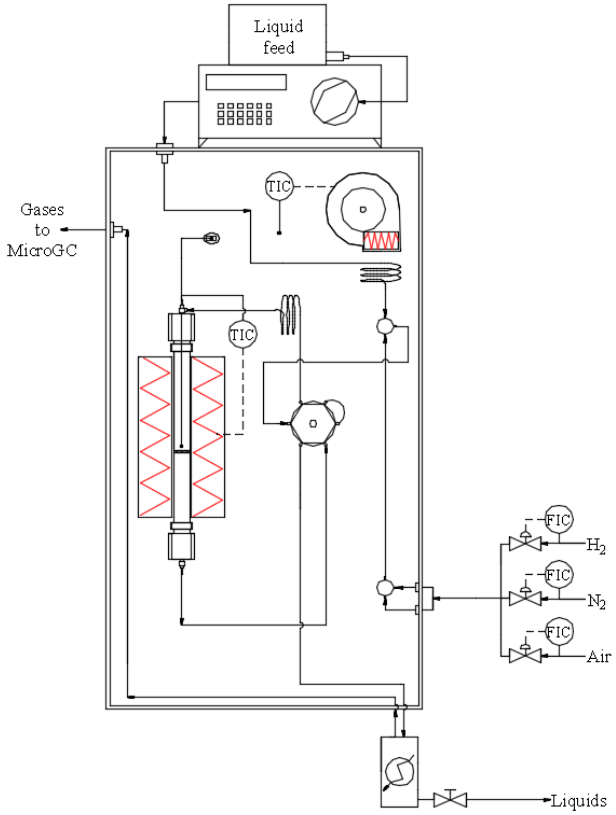

Figure 10. Schematic diagram of the testing system [55].

The outlet gas composition is measured online using an Agilent 490 Micro-GC equipped with a thermal conductivity detector (TCD), a Pora Plot U column (10 m), and a Molecular Sieve 5A column (20 m) using He and Ar as the carrier gas, respectively. Condensable vapors were trapped in the condenser and subsequently analyzed in a Varian CP-3900 chromatograph equipped with a CP-WAX 52 CB column and flame ionization detector (FID), using 1,4-butanediol as an internal standard.

The catalytic performances were compared in terms of acetic acid conversion (X_{AcOH}) and hydrogen yield (Y_{H2}) using Equations (2) and (3), respectively, where n represents the molar flow of acetic acid or hydrogen at the inlet or outlet stream of the reactor.

$$X_{AcOH} = \frac{n_{AcOH,in} - n_{AcOH,out}}{n_{AcOH,in}} \cdot 100 \quad (2)$$

$$Y_{H_2} = \frac{n_{H_2,out}}{4 \cdot n_{AcOH,in}} \cdot 100 \quad (3)$$

The value of carbon deposited during the reaction is reported according to the following expression:

$$Coke\left(mg_{coke} \cdot g_{cat}{}^{-1} \cdot h^{-1}\right) = \frac{m_{coke}(mg)}{m_{catalyst}(g) \cdot TOS(h)} \cdot 100 \quad (4)$$

where m_{coke} is the amount of coke formed during the reaction determined by TGA, and $m_{catalyst}$ is the amount of fresh catalyst introduced into the reactor.

4. Conclusions

Hydrogen production using different Ni catalysts supported on CeO_2-based materials through the oxidative steam reforming of acetic acid as a bio-oil aqueous fraction model compound has been studied for the first time.

First, the effect of the O_2/AcOH molar ratio was studied over Ni/CeO_2. The results evidenced that by increasing the oxygen content, the acetic acid conversion increased along with a decrease in coke deposition and hydrogen yield. To get high acetic acid conversion and hydrogen yield with lower coke deposition, an O_2/AcOH molar ratio = 0.075 was selected.

Three nickel catalysts supported on Ce-based material (commercial CeO_2, a mesostructured CeO_2, and CeO_2-SBA-15) were used in the oxidative steam reforming of acetic acid. As a consequence of better metallic dispersion on the mesostructured CeO_2 and the CeO_2-modified SBA-15 samples, the corresponding catalysts reached conversions 27% and 17% higher than the nonporous Ni/CeO_2, respectively, with an increase of about 25 and 15%, respectively, of hydrogen yield after 5 h TOS. On the other hand, coke deposition was lower with the catalysts prepared over CeO_2 (both commercial and mesostructured) because of the intimate contact of Ni with CeO_2, which favors the oxygen mobility toward carbon gasification. As observed by XRD, in Ni/CeO_2-SBA-15, ceria was deposited as particles, not being completely dispersed over the support; thus, the contact between Ni particles and CeO_2 is less likely to take place. For that reason, coke deposition over Ni/CeO_2-SBA-15 was almost two times higher compared to the other samples, which, along with the active phase oxidation detected by XRD, could explain the conversion drop when using this sample.

In conclusion, the mesostructured Ni/CeO_2_m catalyst achieved almost complete conversion of acetic acid (>97%) and values of hydrogen yield (~52%) close to the predicted by the thermodynamic equilibrium along with the lowest carbon deposition (120.6 $mg_{coke} \cdot g_{cat}{}^{-1} \cdot h^{-1}$) after 5 h TOS at 500 °C. These results evidence that the mesostructured ceria obtained from SBA-15 by nanocasting can be an interesting support for oxidative steam reforming catalysts.

Author Contributions: Conceptualization, A.J.V. and A.C.; methodology, P.J.M. and A.M.; validation, J.A.C., A.J.V. and A.C.; formal analysis, A.J.V. and P.J.M.; investigation, P.J.M. and A.M.; resources, A.C. and J.A.C.; data curation, P.J.M. and A.J.V.; writing—original draft preparation, P.J.M.; writing—review and editing, J.A.C., A.J.V., P.J.M. and A.C.; visualization, A.C. and A.J.V.; supervision J.A.C. and A.C.; project administration, A.C., P.J.M. and J.A.C.; funding acquisition, A.C., P.J.M. and J.A.C. All authors have read and agreed to the published version of the manuscript.

Funding: This research was funded by the Community of Madrid in the framework of the Multiannual Agreement with the Rey Juan Carlos University in line of action 1, "Encouragement of Young Phd students investigation" Project Ref. M2743 with the acronym HYDROGREFOX, by the Community of Madrid with the project S2018/EMT-4344, and the Spanish Ministry for Science and Innovation with the project PID2020-117273RB-I00.

Data Availability Statement: Not applicable.

Conflicts of Interest: The authors declare no conflict of interest.

References

1. Megía, P.J.; Vizcaíno, A.J.; Calles, J.A.; Carrero, A. Hydrogen Production Technologies: From Fossil Fuels toward Renewable Sources. A Mini Review. *Energy Fuels* **2021**, *35*, 16403–16415. [CrossRef]
2. Qureshi, F.; Yusuf, M.; Kamyab, H.; Vo, D.V.N.; Chelliapan, S.; Joo, S.W.; Vasseghian, Y. Latest eco-friendly avenues on hydrogen production towards a circular bioeconomy: Currents challenges, innovative insights, and future perspectives. *Renew. Sustain. Energy Rev.* **2022**, *168*, 112916. [CrossRef]
3. *International Energy Agency (IEA) The Future of Hydrogen*; International Energy Agency: Paris, France, 2019.
4. Capurso, T.; Stefanizzi, M.; Torresi, M.; Camporeale, S.M. Perspective of the role of hydrogen in the 21st century energy transition. *Energy Convers. Manag.* **2022**, *251*, 114898. [CrossRef]
5. International Energy Agency. *World Energy Outlook 2021*; International Energy Agency: Paris, France, 2021.
6. Lepage, T.; Kammoun, M.; Schmetz, Q.; Richel, A. Biomass-to-hydrogen: A review of main routes production, processes evaluation and techno-economical assessment. *Biomass Bioenergy* **2021**, *144*, 105920. [CrossRef]
7. Pal, D.B.; Singh, A.; Bhatnagar, A. A review on biomass based hydrogen production technologies. *Int. J. Hydrogen Energy* **2022**, *47*, 1461–1480. [CrossRef]
8. Nabgan, W.; Tuan Abdullah, T.A.; Mat, R.; Nabgan, B.; Gambo, Y.; Ibrahim, M.; Ahmad, A.; Jalil, A.A.; Triwahyono, S.; Saeh, I. Renewable hydrogen production from bio-oil derivative via catalytic steam reforming: An overview. *Renew. Sustain. Energy Rev.* **2017**, *79*, 347–357. [CrossRef]

9. García-Gómez, N.; Valecillos, J.; Valle, B.; Remiro, A.; Bilbao, J.; Gayubo, A.G. Combined effect of bio-oil composition and temperature on the stability of Ni spinel derived catalyst for hydrogen production by steam reforming. *Fuel* **2022**, *326*, 124966. [CrossRef]
10. Soria, M.A.; Barros, D.; Madeira, L.M. Hydrogen production through steam reforming of bio-oils derived from biomass pyrolysis: Thermodynamic analysis including in situ CO^2 and/or H^2 separation. *Fuel* **2019**, *244*, 184–195. [CrossRef]
11. Kalogiannis, K.G.; Stefanidis, S.D.; Lappas, A.A. Catalyst deactivation, ash accumulation and bio-oil deoxygenation during ex situ catalytic fast pyrolysis of biomass in a cascade thermal-catalytic reactor system. *Fuel Process. Technol.* **2019**, *186*, 99–109. [CrossRef]
12. Gutiérrez Ortiz, F.J.; Kruse, A.; Ramos, F.; Ollero, P. Integral energy valorization of municipal solid waste reject fraction to biofuels. *Energy Convers. Manag.* **2019**, *180*, 1167–1184. [CrossRef]
13. Remón, J.; Broust, F.; Volle, G.; García, L.; Arauzo, J. Hydrogen production from pine and poplar bio-oils by catalytic steam reforming. Influence of the bio-oil composition on the process. *Int. J. Hydrogen Energy* **2015**, *40*, 5593–5608. [CrossRef]
14. Megía, P.J.; Vizcaíno, A.J.; Ruiz-Abad, M.; Calles, J.A.; Carrero, A. Coke evolution in simulated bio-oil aqueous fraction steam reforming using Co/SBA-15. *Catal. Today* **2021**, *367*, 145–152. [CrossRef]
15. Cortese, M.; Ruocco, C.; Palma, V.; Megía, P.J.; Carrero, A.; Calles, J.A. On the Support Effect and the Cr Promotion of Co Based Catalysts for the Acetic Acid Steam Reforming. *Catalysts* **2021**, *11*, 133. [CrossRef]
16. Lopez, G.; Garcia, I.; Arregi, A.; Santamaria, L.; Amutio, M.; Artetxe, M.; Bilbao, J.; Olazar, M. Thermodynamic assessment of the oxidative steam reforming of biomass fast pyrolysis volatiles. *Energy Convers. Manag.* **2020**, *214*, 112889. [CrossRef]
17. Yusuf, M.; Bazli, L.; Alam, M.A.; Masood, F.; Keong, L.K.; Noor, A.; Hellgardt, K.; Abdullah, B. Hydrogen production via natural gas reforming: A comparative study between DRM, SRM and BRM techniques. In Proceedings of the 2021 Third International Sustainability and Resilience Conference: Climate Change, Sakheer, Bahrain, 15–16 November 2021; pp. 155–158. [CrossRef]
18. Ruocco, C.; Palma, V.; Ricca, A. Experimental and kinetic study of oxidative steam reforming of ethanol over fresh and spent bimetallic catalysts. *Chem. Eng. J.* **2019**, *377*, 119778. [CrossRef]
19. Moreira, R.; Bimbela, F.; Gandía, L.M.; Ferreira, A.; Sánchez, J.L.; Portugal, A. Oxidative steam reforming of glycerol. A review. *Renew. Sustain. Energy Rev.* **2021**, *148*, 111299. [CrossRef]
20. Nahar, G.; Dupont, V. Recent advances in hydrogen production via autothermal reforming process (ATR): A review of patents and research articles. *Recent Pat. Chem. Eng.* **2013**, *6*, 8–42. [CrossRef]
21. Ekeoma, B.C.; Yusuf, M.; Johari, K.; Abdullah, B. Mesoporous silica supported Ni-based catalysts for methane dry reforming: A review of recent studies. *Int. J. Hydrogen Energy* **2022**, *148*, 111299. [CrossRef]
22. Matus, E.; Sukhova, O.; Ismagilov, I.; Kerzhentsev, M.; Stonkus, O.; Ismagilov, Z. Hydrogen Production through Autothermal Reforming of Ethanol: Enhancement of Ni Catalyst Performance via Promotion. *Energies* **2021**, *14*, 5176. [CrossRef]
23. Anil, S.; Indraja, S.; Singh, R.; Appari, S.; Roy, B. A review on ethanol steam reforming for hydrogen production over Ni/Al^2O^3 and Ni/CeO^2 based catalyst powders. *Int. J. Hydrogen Energy* **2022**, *47*, 8177–8213. [CrossRef]
24. Xie, X.; Zhou, Q.; Hu, X.; Jia, X.; Huang, L. Zn-Al hydrotalcite-derived $Co_xZn_yAlO_z$ catalysts for hydrogen generation by auto-thermal reforming of acetic acid. *Int. J. Energy Res.* **2019**, *43*, 7075–7084. [CrossRef]
25. Greluk, M.; Rotko, M.; Turczyniak-Surdacka, S. Enhanced catalytic performance of La^2O^3 promoted Co/CeO^2 and Ni/CeO^2 catalysts for effective hydrogen production by ethanol steam reforming. *Renew. Energy* **2020**, *155*, 378–395. [CrossRef]
26. Wang, H.; Zhu, H.; Zhang, Y.; Pu, J. Highly active Ni/CeO^2 for the steam reforming of acetic acid using CTAB as surfactant template. *Int. J. Hydrogen Energy* **2022**, *47*, 27493–27507. [CrossRef]
27. Lykaki, M.; Pachatouridou, E.; Carabineiro, S.A.C.; Iliopoulou, E.; Andriopoulou, C.; Kallithrakas-Kontos, N.; Boghosian, S.; Konsolakis, M. Ceria nanoparticles shape effects on the structural defects and surface chemistry: Implications in CO oxidation by Cu/CeO^2 catalysts. *Appl. Catal. B Environ.* **2018**, *230*, 18–28. [CrossRef]
28. Vizcaíno, A.J.; Carrero, A.; Calles, J.A. Hydrogen production by ethanol steam reforming over Cu–Ni supported catalysts. *Int. J. Hydrogen Energy* **2007**, *32*, 1450–1461. [CrossRef]
29. Sing, K.S.W.; Everett, D.H.; Haul, R.A.W.; Moscou, L.; Pierotti, R.A.; Rouquerol, J.; Siemieniewska, T. Reporting Physisorption Data for Gas/Solid Systems with Special Reference to the Determination of Surface Area and Porosity. *Pure Appl. Chem.* **1985**, *57*, 603–619. [CrossRef]
30. Megía, P.J.; Carrero, A.; Calles, J.A.; Vizcaíno, A.J. Hydrogen Production from Steam Reforming of Acetic Acid as a Model Compound of the Aqueous Fraction of Microalgae HTL Using Co-M/SBA-15 (M: Cu, Ag, Ce, Cr) Catalysts. *Catalysts* **2019**, *9*, 1013. [CrossRef]
31. Roggenbuck, J.; Schäfer, H.; Tsoncheva, T.; Minchev, C.; Hanss, J.; Tiemann, M. Mesoporous CeO^2: Synthesis by nanocasting, characterisation and catalytic properties. *Microporous Mesoporous Mater.* **2007**, *101*, 335–341. [CrossRef]
32. Luo, L.; Oliver, C.C.; Joseph, I.M.; Gang, D.D.; Chen, M.; Hernandez, R.; Yan, H. Pore structure of ordered mesoporous $Pt\text{-}CeO^2$ probed by CO via VT-DRIFTS. *Appl. Surf. Sci.* **2022**, *588*, 152866. [CrossRef]
33. Calles, J.A.; Carrero, A.; Vizcaíno, A.J. Ce and La modification of mesoporous Cu–Ni/SBA-15 catalysts for hydrogen production through ethanol steam reforming. *Microporous Mesoporous Mater.* **2009**, *119*, 200–207. [CrossRef]
34. Sepehri, S.; Rezaei, M.; Wang, Y.; Younesi, A.; Arandiyan, H. The evaluation of autothermal methane reforming for hydrogen production over Ni/CeO^2 catalysts. *Int. J. Hydrogen Energy* **2018**, *43*, 22340–22346. [CrossRef]
35. Ferreira, G.R.; Nogueira, F.G.E.; Lucrédio, A.F.; Assaf, E.M. Ethanol Steam Reforming by Ni Catalysts for H^2 Production: Evaluation of Gd Effect in CeO^2 Support. *Catal. Lett.* **2022**, *152*, 3125–3145. [CrossRef]

36. Calles, J.A.; Carrero, A.; Vizcaíno, A.J.; García-Moreno, L.; Megía, P.J. Steam Reforming of Model Bio-Oil Aqueous Fraction Using Ni-(Cu, Co, Cr)/SBA-15 Catalysts. *Int. J. Mol. Sci.* **2019**, *20*, 512. [CrossRef] [PubMed]
37. Megía, P.J.; Calles, J.A.; Carrero, A.; Vizcaíno, A.J. Effect of the incorporation of reducibility promoters (Cu, Ce, Ag) in Co/CaSBA-15 catalysts for acetic acid steam reforming. *Int. J. Energy Res.* **2021**, *45*, 1685–1702. [CrossRef]
38. Scheffe, J.R.; Steinfeld, A. Thermodynamic analysis of cerium-based oxides for solar thermochemical fuel production. *Energy Fuels* **2012**, *26*, 1928–1936. [CrossRef]
39. Batista da Silva, R.; Brandão, S.T.; Lucotti, A.; Tommasini, M.S.; Castiglioni, C.; Groppi, G.; Beretta, A. Chemical pathways in the partial oxidation and steam reforming of acetic acid over a Rh-Al^2O^3 catalyst. *Catal. Today* **2017**, *289*, 162–172. [CrossRef]
40. Osorio-Vargas, P.; Flores-González, N.A.; Navarro, R.M.; Fierro, J.L.G.; Campos, C.H.; Reyes, P. Improved stability of Ni/Al^2O^3 catalysts by effect of promoters (La^2O^3, CeO^2) for ethanol steam-reforming reaction. *Catal. Today* **2016**, *259*, 27–38. [CrossRef]
41. Bereketidou, O.A.; Goula, M.A. Biogas reforming for syngas production over nickel supported on ceria–alumina catalysts. *Catal. Today* **2012**, *195*, 93–100. [CrossRef]
42. Santos, A.C.S.F.; Damyanova, S.; Teixeira, G.N.R.; Mattos, L.V.; Noronha, F.B.; Passos, F.B.; Bueno, J.M.C. The effect of ceria content on the performance of Pt/CeO^2/Al^2O^3 catalysts in the partial oxidation of methane. *Appl. Catal. A Gen.* **2005**, *290*, 123–132. [CrossRef]
43. Trimm, D.L. Coke formation and minimisation during steam reforming reactions. *Catal. Today* **1997**, *37*, 233–238. [CrossRef]
44. Ruocco, C.; Palma, V.; Ricca, A. Hydrogen production by oxidative reforming of ethanol in a fluidized bed reactor using a PtNi/CeO^2SiO^2 catalyst. *Int. J. Hydrogen Energy* **2019**, *44*, 12661–12670. [CrossRef]
45. Lima, D.S.; Calgaro, C.O.; Perez-Lopez, O.W. Hydrogen production by glycerol steam reforming over Ni based catalysts prepared by different methods. *Biomass Bioenergy* **2019**, *130*, 105358. [CrossRef]
46. Zhao, D.; Feng, J.; Huo, Q.; Melosh, N.; Fredrickson, G.H.; Chmelka, B.F.; Stucky, G.D. Triblock copolymer syntheses of mesoporous silica with periodic 50 to 300 angstrom pores. *Science* **1998**, *279*, 548–552. [CrossRef] [PubMed]
47. Lolli, A.; Amadori, R.; Lucarelli, C.; Cutrufello, M.G.; Rombi, E.; Cavani, F.; Albonetti, S. Hard-template preparation of Au/CeO^2mesostructured catalysts and their activity for the selective oxidation of 5-hydroxymethylfurfural to 2,5-furandicarboxylic acid. *Microporous Mesoporous Mater.* **2016**, *226*, 466–475. [CrossRef]
48. Deeprasertkul, C.; Longloilert, R.; Chaisuwan, T.; Wongkasemjit, S. Impressive low reduction temperature of synthesized mesoporous ceria via nanocasting. *Mater. Lett.* **2014**, *130*, 218–222. [CrossRef]
49. Gu, D.; Schüth, F. Synthesis of non-siliceous mesoporous oxides. *Chem. Soc. Rev.* **2014**, *43*, 313–344. [CrossRef]
50. Deng, X.; Chen, K.; Tüysüz, H. Protocol for the Nanocasting Method: Preparation of Ordered Mesoporous Metal Oxides. *Chem. Mater.* **2017**, *29*, 40–52. [CrossRef]
51. Xiao, W.; Yang, S.; Zhang, P.; Li, P.; Wu, P.; Li, M.; Chen, N.; Jie, K.; Huang, C.; Zhang, N.; et al. Facile Synthesis of Highly Porous Metal Oxides by Mechanochemical Nanocasting. *Chem. Mater.* **2018**, *30*, 2924–2929. [CrossRef]
52. Martinez-Diaz, D.; Martínez del Monte, D.; García-Rojas, E.; Alique, D.; Calles, J.A.; Sanz, R. Comprehensive permeation analysis and mechanical resistance of electroless pore-plated Pd-membranes with ordered mesoporous ceria as intermediate layer. *Sep. Purif. Technol.* **2021**, *258*, 118066. [CrossRef]
53. Li, H.; Jia, X.; Wang, N.; Chen, B.; Xie, X.; Wang, Q.; Huang, L. Auto-thermal reforming of acetic acid over hydrotalcites-derived co-based catalyst: A stable and anti-coking Co/Sr-Alx-O catalyst. *Appl. Catal. B Environ.* **2020**, *267*, 118370. [CrossRef]
54. Hu, X.; Yang, J.; Sun, W.; Wang, N.; An, S.; Wang, Q.; Zhang, Y.; Xie, X.; Huang, L. Y-Zr-O solid solution supported Ni-based catalysts for hydrogen production via auto-thermal reforming of acetic acid. *Appl. Catal. B Environ.* **2020**, *278*, 119264. [CrossRef]
55. Carrero, A.; Calles, J.A.; García-Moreno, L.; Vizcaíno, A.J. Production of renewable hydrogen from glycerol steam reforming over bimetallic Ni-(Cu,Co,Cr) catalysts supported on SBA-15 silica. *Catalysts* **2017**, *7*, 55. [CrossRef]